

Multiconfigurational Theoretical Study of the Octamethyldimetalates of Cr(II), Mo(II), W(II), and Re(III): Revisiting the Correlation between the M–M Bond Length and the $\delta \rightarrow \delta^*$ Transition Energy

Francesco Ferrante,[†] Laura Gagliardi,[†] Bruce E. Bursten,^{‡,||} and Alfred P. Sattelberger[§]

Dipartimento di Chimica Fisica “F. Accascina,” Università di Palermo, Viale delle Scienze-Parco d’Orleans II, I-90128 Palermo, Italy, Department of Chemistry, The Ohio State University, 100 West 18th Avenue, Columbus, Ohio 43210, and Chemistry Division, Los Alamos National Laboratory, Los Alamos, New Mexico 87545

Received March 18, 2005

Four compounds containing metal–metal quadruple bonds, the $[M_2(CH_3)_8]^{n-}$ ions ($M = Cr, Mo, W, Re$ and $n = 4, 4, 4, 2$, respectively), have been studied theoretically using multiconfigurational quantum-chemical methods. The molecular structure of the ground state of these compounds has been determined and the energy of the $\delta \rightarrow \delta^*$ transition has been calculated and compared with previous experimental measurements. The high negative charges on the Cr, Mo, and W complexes lead to difficulties in the successful modeling of the ground-state structures, a problem that has been addressed by the explicit inclusion of four Li^+ ions in these calculations. The ground-state geometries of the complexes and the $\delta \rightarrow \delta^*$ transition have been modeled with either excellent agreement with experiment (Re) or satisfactory agreement (Cr, Mo, and W).

Introduction

In 1965, Cotton and Harris reported the crystal structure of $K_2[Re_2Cl_8] \cdot 2H_2O$.¹ The surprisingly short Re–Re distance of 2.24 Å, the eclipsed conformation of the $ReCl_4$ fragments, and the diamagnetism of the complex led to the recognition of the first quadruple metal–metal bond.² The discovery of the quadruple Re–Re bond in $[Re_2Cl_8]^{2-}$ led to a new era in inorganic chemistry, and since then, hundreds of compounds containing multiple metal–metal bonds have been characterized.³

The well-known qualitative description of the quadruple bond in $d^4-d^4 M_2X_8$ complexes is elegant and deceptively simple. In a molecular orbital description of the multiple bonding, the electron count and the eclipsed D_{4h} geometry

facilitate the occupation of $d\sigma$, doubly degenerate $d\pi$, and $d\delta$ metal–metal bonding molecular orbitals (MOs). The $d\delta$ MO, which, in the usual coordinate system involves the interaction of “face-to-face” d_{xy} atomic orbitals on the two metal centers, provides a particular challenge to quantitative electronic-structure calculations. The small overlap between the orbitals and the resultant, relatively weak, interaction makes a simple MO description of the quadruple bond inappropriate.⁴ Indeed, the proper description of the quadruple bond requires an approach that goes beyond the single-configuration approach inherent to simple MO formalisms.

The most common metrics used to gauge the quality of quantitative calculations of the electronic structure of quadruple bonds are the metal–metal bond distance and the $\delta \rightarrow \delta^*$ (${}^1A_{2u} \leftarrow {}^1A_{1g}$ under D_{4h} symmetry) excitation energy. The latter quantity is particularly challenging to calculate because of the sensitivity of the ground and excited states to electron correlation. One of us recently studied the structure and electronic spectrum of $[Re_2Cl_8]^{2-}$ using multiconfigurational quantum chemistry,⁵ an approach that includes the electron correlation necessary to properly describe the complexity of the multiple bond. The same

* To whom correspondence should be addressed. E-mail: laura.gagliardi@unipa.it.

[†] Università di Palermo.

[‡] The Ohio State University.

^{||} Present address: The University of Tennessee, 26 Alumni Memorial Building, Knoxville, TN 37996-1320.

[§] Los Alamos National Laboratory.

(1) (a) Cotton, F. A.; Harris, C. B. *Inorg. Chem.* **1965**, *4*, 330. (b) Cotton, F. A.; Curtis, N. F.; Harris, B. F.; Johnson, B. F. G.; Lippard, S. J.; Mague, J. T.; Robinson, W. R.; Wood, J. S. *Science* **1964**, *145*, 1305.

(2) Cotton, F. A. *Inorg. Chem.* **1965**, *4*, 334.

(3) Cotton, F. A.; Walton, R. A. *Multiple Bonds Between Metal Atoms*, 2nd ed.; Clarendon: Oxford, U.K., 1993.

(4) (a) Bursten, B. E.; Clayton, T. W., Jr. *J. Cluster Sci.* **1994**, *5*, 157. (b) Cotton, F. A.; Nocera, D. G. *Acc. Chem. Res.* **2000**, *33*, 483.

(5) Gagliardi, L.; Roos, B. *Inorg. Chem.* **2003**, *42*, 1599.

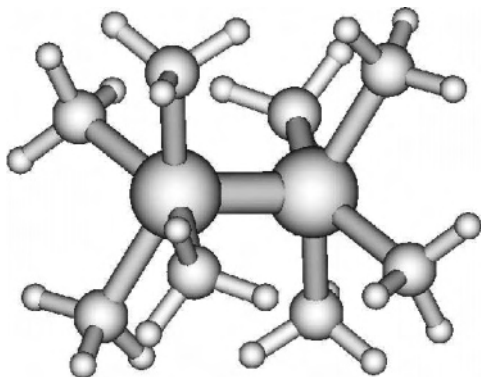


Figure 1. Structure of $\text{Cr}_2(\text{CH}_3)_8^{4-}$, $\text{Mo}_2(\text{CH}_3)_8^{4-}$, $\text{W}_2(\text{CH}_3)_8^{4-}$, and $\text{Re}_2(\text{CH}_3)_8^{2-}$.

approach had earlier been used to describe successfully the properties and electronic spectrum of the Cr_2 molecule,^{6–8} which formally has a sextuple bond, and dichromium tetraformate.⁹

The most commonly studied compounds with quadruple bonds contain halide ligands or unsaturated bridging ligands, such as carboxylates or, more recently, novel heteroatom-containing ligands such as formamidinates.¹⁰ These ligands actually complicate the description of the δ bonding because they can serve as π donors that can interact with the δ and δ^* orbitals. In principle, the simplest M_2X_8 system, with respect to description of the δ interactions, would involve X ligands that are σ donors only; such ligands are, by symmetry, unable to interact with the δ and δ^* orbitals. The simplest real quadruply bonded systems that contain σ -only ligands are the $[\text{M}_2(\text{CH}_3)_8]^{n-}$ complexes that are the focus of the present study.

Several years ago, one of us reported an experimental study on the electronic spectra of the d^4 – d^4 octamethyldimetalates of Cr(II), Mo(II), and Re(III) (Figure 1), a set that encompasses all three transition-metal series.¹¹

A near-linear correlation was observed between the $\delta \rightarrow \delta^*$ transition energy and the metal–metal bond length, which seemed all the more surprising given that compounds from all three rows of the transition metals were included. The $\delta \rightarrow \delta^*$ transition energy increases as the metal–metal bond length decreases from Re to Mo to Cr, an indication that both observables are sensitive in a similar way to the overlap of the d_{xy} orbitals. Somewhat surprisingly, the correlation between metal–metal bond length and the $\delta \rightarrow \delta^*$ transition energy in these octamethyldimetalates has received no subsequent experimental or computational study. In this paper, we report the results of a comprehensive quantum chemical study of this series of complexes, together with $[\text{W}_2(\text{CH}_3)_8]^{4-}$, which has been studied experimentally by Collins et al.¹² The ground-state structures of the

complexes have been calculated, along with the $\delta \rightarrow \delta^*$ transition energies and intensities.

Details of the Calculations

The study was performed using the complete active space (CAS) SCF method¹³ with dynamic correlation added by multiconfigurational second-order perturbation theory (CASPT2).^{14–16} Scalar relativistic effects were included via a Douglas–Kroll (DK) Hamiltonian.^{17,18} The effects of spin–orbit (SO) coupling were not taken into account; the previous calculations on $[\text{Re}_2\text{Cl}_8]^{2-}$ demonstrated that SO effects did not significantly affect the electronic spectrum in the energy region in the vicinity of the ground state.⁵ All calculations have been performed with the software MOLCAS, version 6.0.¹⁹

Newly developed basis sets have been used for all atoms.²⁰ They are of the atomic natural orbital (ANO) type with the expansion coefficients optimized in CASSCF/CASPT2 calculations on different spectroscopic states of the atom and positive ion. The DK Hamiltonian was used to include scalar relativistic effects. We note that such a basis set can only be used in relativistic calculations. For Re, the primitive set 24s20p15d11f3g was contracted to 8s7p5d3f1g. The same basis set was used in our previous study on $[\text{Re}_2\text{Cl}_8]^{2-}$,⁵ for which it gave satisfactory agreement with the experimental results. For Cr, Mo, and W, the primitive sets 21s15p10d6f4g, 21s15p10d6f4g, and 24s21p15d11f4g2h were contracted to 6s5p3d2f1g, 7s6p4d2f1g, and 8s7p5d3f1g, respectively. For the light atoms, C and H, the primitive basis set was contracted to 4s3p2d1f and 2s1p, respectively. For the Li atom, a ANO basis set contracted to 3s functions was used.

The geometry of the ground state of the four complexes was initially taken from crystallographic data.^{12,21} A numerical optimization of two degrees of freedom of the complexes, the metal–metal, M–M, and metal–carbon, M–C, bond distances was then performed at the CASPT2 level, assuming that the complexes had D_{4h} symmetry. Because MOLCAS works in subgroups of the D_{2h} point group, all calculations were performed in this symmetry. The numerical optimization gave a bound structure for $[\text{Re}_2(\text{CH}_3)_8]^{2-}$, while the highly negatively charged $[\text{Cr}_2(\text{CH}_3)_8]^{4-}$, $[\text{Mo}_2(\text{CH}_3)_8]^{4-}$,

- (6) Andersson, K. *Chem. Phys. Lett.* **1995**, *237*, 212.
 (7) Roos, B. O. *Collect. Czech. Chem. Commun.* **2003**, *68*, 265.
 (8) Cotton, F. A. *Polyhedron* **1987**, *6*, 667.
 (9) Andersson, K.; Bauschlicher, C. W., Jr.; Persson, B. J.; Roos, B. O. *Chem. Phys. Lett.* **1996**, *257*, 238.
 (10) For example, see: Cotton, F. A.; Lin, C.; Murillo, C. A. *Acc. Chem. Res.* **2001**, *34*, 759.
 (11) Sattelberger, A. P.; Fackler, J. P. *J. Am. Chem. Soc.* **1977**, *99*, 1258.

- (12) Collins, D. M.; Cotton, F. A.; Kock, S.; Millar, M.; Murillo, C. A. *J. Am. Chem. Soc.* **1977**, *99*, 1259.
 (13) Roos, B. O. In *Advances in Chemical Physics: Ab Initio Methods in Quantum Chemistry II*; Lawley, K. P., Ed.; John Wiley & Sons Ltd.: Chichester, U. K., 1987; p 399.
 (14) Andersson, K.; Malmqvist, P.-A.; Roos, B. O.; Sadlej, A. J.; Wolinski, K. *J. Phys. Chem.* **1990**, *94*, 5483.
 (15) Andersson, K.; Malmqvist, P.-A.; Roos, B. O. *J. Chem. Phys.* **1992**, *96*, 1218.
 (16) Roos, B. O.; Andersson, K.; Fiilscher, M. P.; Malmqvist, P.-Å.; Serrano-Andres, L.; Pierloot, K.; Merchan, M. In *Advances in Chemical Physics: New Methods in Computational Quantum Mechanics*; Prigogine, I., Rice, S. A., Eds.; John Wiley & Sons: New York, 1996; Vol. XCIII, pp 219–331.
 (17) Douglas, N.; Kroll, N. M. *Ann. Phys.* **1974**, *82*, 89.
 (18) Hess, B. *Phys. Rev. A* **1986**, *33*, 3742.
 (19) Andersson, K.; Barysz, M.; Bernhardsson, A.; Blomberg, M. R. A.; Carissan, Y.; Cooper, D. L.; Fulscher, M. P.; Gagliardi, L.; de Graaf, C.; Hess, B. A.; Karlstrom, G.; Lindh, R.; Malmqvist, P.-A.; Nakajima, T.; Neogrady, P.; Olsen, J.; Roos, B. O.; Schimmelpfennig, B.; Schutz, M.; Seijo, L.; Serrano-Andres, L.; Siegbahn, P. E. M.; Stalring, J.; Thorsteinsson, T.; Veryazov, V.; Widmark, P.-O. *MOLCAS*, version 6.0; Department of Theoretical Chemistry, Chemistry Center, University of Lund: Lund, Sweden, 2003.
 (20) Roos, B. O.; Widmark, P.-O. To be published.
 (21) (a) For Cr, see: Krause, J.; Marx, G.; Schödl, G. *J. Organomet. Chem.* **1970**, *21*, 159. (b) For Mo, see: Cotton, F. A.; Troup, J. M.; Webb, T. R.; Williamson, D. H.; Wilkinson, G. *J. Am. Chem. Soc.* **1974**, *96*, 3824. (c) For Re, see: Cotton, F. A.; Gage, L. D.; Mertis, K.; Shive, L. W.; Wilkinson, G. *J. Am. Chem. Soc.* **1978**, *98*, 6922.

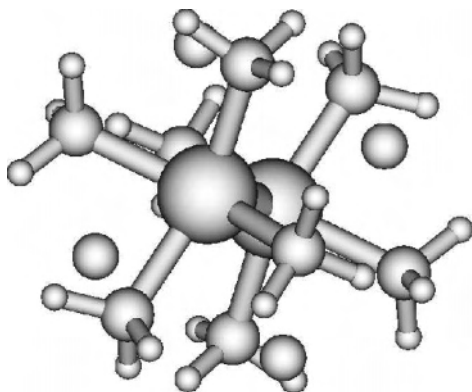


Figure 2. Structure of $\text{Cr}_2(\text{CH}_3)_8\text{Li}_4$, $\text{Mo}_2(\text{CH}_3)_8\text{Li}_4$, and $\text{W}_2(\text{CH}_3)_8\text{Li}_4$.

Table 1. Experimental and CASPT2 Bond Distances (Å), Angles (deg), and $\delta \rightarrow \delta^*$ Vertical ($^1A_{1g}$) and Adiabatic ($^1A_{2u}$) Excitation Energies (eV) for the $[\text{M}_2(\text{CH}_3)_8]^{n-}$ Species

system	$R_{\text{M-M}}$	$R_{\text{M-C}}$	$\angle \text{M-M-C}$	$R_{\text{M-Li}}$	$\Delta E (\delta \rightarrow \delta^*)^a$
$\text{Li}_4[\text{Cr}_2(\text{CH}_3)_8]$					
exptl	1.980	2.199	107.0	2.558	2.73
CASPT2 $^1A_{1g}$	2.041	2.239	"	"	3.02 (0.005)
CASPT2 $^1A_{2u}$	2.165	2.218	"	"	2.95
$\text{Li}_4[\text{Mo}_2(\text{CH}_3)_8]$					
exptl	2.149	2.282	104.7	2.696	2.41
CASPT2 $^1A_{1g}$	2.191	2.324	"	"	2.77 (0.035)
CASPT2 $^1A_{2u}$	2.280	2.309	"	"	2.66
$\text{Li}_4[\text{W}_2(\text{CH}_3)_8]$					
exptl	2.263	2.20	109	2.619	2.09
CASPT2 $^1A_{1g}$	2.331	2.291	102.7	2.619	2.39 (0.042)
$[\text{Re}_2(\text{CH}_3)_8]^{2-}$					
exptl	2.178	2.19	105.7		2.31
CASPT2 $^1A_{1g}$	2.197	2.232	106.8		2.53 (0.029)

^a Oscillator strength in parentheses.

and $[\text{W}_2(\text{CH}_3)_8]^{4-}$ ions turned out to be unbound. The optimizations of these tetraanions were then performed in the presence of four Li^+ counterions placed in the plane perpendicular to the M–M bond (Figure 2) to maintain D_{4h} symmetry.

The choice of the active space is the crucial step in a CASSCF/CASPT2 calculation. The procedure followed in our previous study on $[\text{Re}_2\text{Cl}_8]^{2-}$ has also been employed in this study. An active space formed by twelve electrons in twelve active orbitals (12/12) was used. This space is composed of one $5d\sigma$, two $5d\pi$, and one $5d\delta$ M–M bonding orbitals and the corresponding antibonding orbitals and two M–C δ bonding orbitals and the corresponding antibonding orbitals. This space does not contain the full atomic d shell. Preliminary investigations on selected systems indicated that a larger active space, with the full d shell, would give results analogous to those obtained with the 12/12 active space. We thus decided to use the 12/12 active space for all the systems. This active space can only describe electronic states where the excitations are localized within the M–M bond. A more extensive active space would be needed to calculate the ligand-to-metal charge-transfer excitations, therefore these excitations have not been considered in the present study.

Results and Discussion

The CASPT2 geometries of the complexes and $\delta \rightarrow \delta^*$ transition energies are reported in Table 1, together with the experimental values.

Inspection of Table 1 shows that in the case of $[\text{Re}_2(\text{CH}_3)_8]^{2-}$, the calculated bond distances reproduce the experimental values better than in the $\text{Li}_4[\text{Cr}_2(\text{CH}_3)_8]$,

$\text{Li}_4[\text{Mo}_2(\text{CH}_3)_8]$, and $\text{Li}_4[\text{W}_2(\text{CH}_3)_8]$ cases. For $[\text{Re}_2(\text{CH}_3)_8]^{2-}$, the same quality of agreement between calculation and experiment was obtained as in the previous study on $[\text{Re}_2\text{Cl}_8]^{2-}$.⁵ The difference between the calculated and experimental Re–Re bond distance is 0.02 Å. The band detected experimentally at 2.31 eV (18 600 cm^{-1}) has been assigned to the $\delta \rightarrow \delta^*$ ($^1A_{2u} \leftarrow ^1A_{1g}$) transition. Our calculation predicts an excitation energy of 2.53 eV with an oscillator strength equal to 0.029. In the case of $[\text{Re}_2\text{Cl}_8]^{2-}$, the experimental band peaks at 1.82 eV with an oscillator strength of 0.023, and the calculated excitation energy is 2.03 eV, with an oscillator strength equal to 0.004. Thus, both calculations on the $[\text{Re}_2\text{X}_8]^{2-}$ (X = Cl, CH₃) systems calculate the key optical transition energy within about 0.2 eV.

As previously mentioned, the $[\text{Cr}_2(\text{CH}_3)_8]^{4-}$, $[\text{Mo}_2(\text{CH}_3)_8]^{4-}$, and $[\text{W}_2(\text{CH}_3)_8]^{4-}$ ions turned out to be unbound at the CASPT2 level, dissociating into two $[\text{M}(\text{CH}_3)_4]^{2-}$ fragments. We tried to optimize the M–M and M–C bond distances using the polarizable continuum model as implemented in MOLCAS, version 6.0, to mimic solvent effects, but the systems still dissociated. The only possible explanation for this behavior that we could find was that the rather simplified dielectric model used was unable to stabilize complexes with such a high negative charge (4[−]). Since the crystal structures of these tetraanions show noninnocent interactions with their cations, we decided to repeat the calculations on the Cr, Mo, and W complexes in the presence of four Li^+ counterions, hoping that doing so would introduce a more realistic model for the actual systems. We therefore optimized the M–M and M–C bond distances for the neutral systems $\text{Li}_4[\text{M}_2(\text{CH}_3)_8]$ in which the four Li^+ ions were sited on the plane perpendicular to the M–M bond at half the M–M distance to maintain D_{4h} symmetry. The distance between the Li^+ ions and the M–M bond was taken from the crystal structures (Figure 2).

In Table 1, the typical bond distances and angles and excitation energy for the Cr, Mo, and W complexes are reported. The CASPT2 bond distances differ significantly from the experimental values. The Cr–C, Mo–C, and W–C calculated bond distances are 0.06, 0.04, and 0.07 Å, respectively, longer than the corresponding experimental values. The calculated excitation energies at the CASPT2 geometries are 0.30, 0.35, and 0.30 eV, respectively, larger than the experimental values (i.e., nearly 50% as large as those in the $[\text{Re}_2\text{X}_8]^{2-}$ systems). We believe that the difficulties in modeling $[\text{Cr}_2(\text{CH}_3)_8]^{4-}$, $[\text{Mo}_2(\text{CH}_3)_8]^{4-}$, and $[\text{W}_2(\text{CH}_3)_8]^{4-}$ are primarily the result of the highly negative charges. We experienced a similar problem in a study of the neptunyl tricarbonate pentaanion, $[\text{NpO}_2(\text{CO}_3)_3]^{5-}$ where it was problematic to reproduce the experimental geometries even in the presence of counterions because of the highly negative charge of the complex.²²

To further explore the effects of the highly negative $[(\text{CH}_3)_8]^{8-}$ ligand field on the calculated structures of $\text{Li}_4[\text{Cr}_2(\text{CH}_3)_8]^{4-}$ and $\text{Li}_4[\text{Mo}_2(\text{CH}_3)_8]^{4-}$, we have also per-

formed constrained-geometry calculations on these systems in which the M–C distances were fixed at those in the crystal structures. Under this constraint, the optimized Cr–Cr and Mo–Mo bond distances are 2.069 and 2.218 Å, respectively. When the constraint is relaxed and the M–C and M–M bond lengths are both optimized, the M–C bonds lengthen and the Cr–Cr and Mo–Mo bonds shorten to 2.041 and 2.191 Å, respectively (Table 1). These observations suggest to us that the four Li^+ counterions may not be adequate to offset the highly negative charge that is largely localized on the CH_3^- ligands. This all seems to indicate that the behavior detected here is typical of insufficient cationic embedding. We are presently considering implementation of methodologies such as the ab initio model potentials (AIMPs) of Barandiarán and Seijo²³ to model the embedding in a more appropriate way and to allow consideration of the interactions with neighboring crystal cells.

Interestingly, the problems encountered in converging the structures of the $[\text{M}_2(\text{CH}_3)_8]^{4-}$ complexes are apparently not encountered for the corresponding chloro complex, $[\text{Mo}_2\text{Cl}_8]^{4-}$, investigated at DFT level.²⁴ We believe this observation indicates that the more electronegative Cl^- ligands can better absorb the effects of the excess electronic charge than can the harder CH_3^- ligands. In fact, it is somewhat surprising that $[\text{Re}_2(\text{CH}_3)_8]^{2-}$ converged so readily; apparently, the greater electrostatic stabilization of the formally Re(III) centers relative to the Cr(II), Mo(II), and W(II) centers is enough to stabilize the structure even in the absence of counterions.

Despite the challenges in calculating the structures of the $[\text{M}_2(\text{CH}_3)_8]^{4-}$ complexes, we still wanted to address the experimentally observed relationship between the metal–metal bond length and the energy of the $\delta \rightarrow \delta^*$ (${}^1\text{A}_{2u} \leftarrow {}^1\text{A}_{1g}$) transition for the Cr, Mo, W, and Re series. In the cases of Cr and Mo, in addition to the vertical excitation energies, we also optimized the metal–metal and metal–carbon distance for the ${}^1\text{A}_{2u}$ excited state and computed the adiabatic excitation energies. In the excited state, the metal–metal bond distance increases, as expected, while the metal–carbon distance decreases, and the adiabatic excitation energy is closer to the experimental value than the vertical excitation energy (Table 1).

Figure 3 shows a plot of the $\delta \rightarrow \delta^*$ excitation energy versus the metal–metal bond distance for the Cr, Mo, Re, and W complexes.

The curve with the squares reports the experimental results. The curve with the circles reports the CASPT2 excitation energies calculated at the experimental geometries, and the curve with the triangles shows the CASPT2 excitation energies calculated at the CASPT2-optimized geometries. The trends in the three curves are similar, in the sense that the $\delta \rightarrow \delta^*$ excitation energy decreases along the series as the metal–metal bond distance increases. The CASPT2 metal–metal distances are longer than the experimental distances, which explains why the CASPT2 excitation ener-

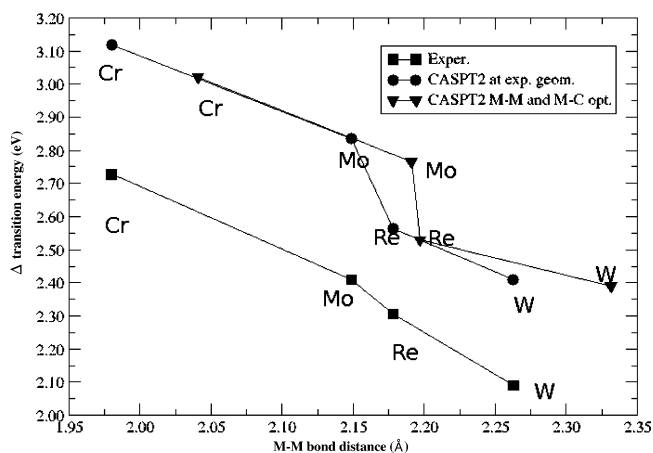


Figure 3. $\delta \rightarrow \delta^*$ (${}^1\text{A}_{2u} \leftarrow {}^1\text{A}_{1g}$) excitation energy (eV) as a function of the metal–metal bond distance (Å) for the Cr, Mo, W, and Re complexes, respectively: experimental data (■), CASPT2 calculations at the experimental geometries (●), and CASPT2 calculations at the CASPT2-optimized geometries (▼).

gies at the CASPT2 geometries are lower than then the CASPT2 excitation energies at the experimental geometries. The experimental curve (squares) is close to a straight line, showing an almost linear correlation between the $\delta \rightarrow \delta^*$ excitation energy and the metal–metal bond length, as pointed out in the experimental papers.^{11,12} The calculated curves, on the other hand, are not linear, indicating a clear difference between the experimental and computational results. If, on the other hand, we considered only the Cr, Mo, and W points, they would also lie on a straight line. This shows that the calculations on the (4−) species are different from the calculations on the (2−) species.

In the original paper,¹¹ the decrease of the excitation energy along the series (Cr to Mo to Re) was ascribed to an increase in the M–M separation and a decrease in the δ overlap. Other factors should also be considered. The molecular orbitals increase in size along the series, and they eventually overlap at a larger distance between the two central atoms. Moreover, the transitions usually become closer in the electronic spectrum of heavier atoms. These factors may also be responsible for the observed trend.

Finally, we analyzed the molecular orbitals and the ground-state wave functions for the four complexes. We shall start the discussion with the $[\text{Re}_2(\text{CH}_3)_8]^{2-}$ complex, given its close similarity to $[\text{Re}_2\text{Cl}_8]^{2-}$.⁵ The dominant electronic configuration in the ${}^1\text{A}_{1g}$ ground state has a weight of 0.71, and the twelve molecular orbitals used in the calculations are nicely paired so that the sum of the occupation numbers for the bonding and antibonding orbitals of a given type is almost exactly two. We note that the two bonding Re–C orbitals are mainly located on C as expected, while the antibonding orbitals have large contributions from the Re $5d_{x^2-y^2}$ orbital. The occupation is low, and these orbitals are thus almost empty and may be used as acceptor orbitals for electronic transitions. The strongest bond between the two Re atoms is the σ bond, with occupation numbers $\eta_b = 1.92$ for the bonding natural orbital and $\eta_a = 0.08$ for the antibonding natural orbital. We can estimate the effective bond order as $(\eta_b - \eta_a)/(\eta_b + \eta_a)$. Thus, for the σ bond we

(23) Barandiarán, Z.; Seijo, L. *J. Chem. Phys.* **1988**, *89*, 5739.

(24) Brett, C. M.; Bursten, B. E. Unpublished results.

obtain the value 0.92. The corresponding value for the π bond is 1.82. The δ/δ^* pair gives an effective bond order of only 0.65. The addition of these numbers results in a total effective bond order of 3.39. A similar analysis for $[\text{Re}_2\text{Cl}_8]^{2-}$ gave an effective bond order of 3.20; the reduction of the bond order from 4.0 to 3.2 was explained principally in terms of the weakness of the δ bond and the concomitant correlation of the δ and δ^* orbitals. In addition, the weakly π -donating Cl^- ligands can donate into the vacant δ^* orbital, increasing its occupancy. Thus, the greater Re–Re bond order in $[\text{Re}_2(\text{CH}_3)_8]^{2-}$ relative to $[\text{Re}_2\text{Cl}_8]^{2-}$ reflects the fact that CH_3^- is a σ -only ligand, although this bond is still closer to a triple than a quadruple bond. The $\text{Li}_4[\text{W}_2(\text{CH}_3)_8]$ species has a similar electronic configuration and orbital occupation.

In $\text{Li}_4[\text{Mo}_2(\text{CH}_3)_8]$, the main electronic configuration has a weight of 0.75 and the effective bond orders for the σ , π , and δ bonds are 0.89, 1.82, and 0.76, respectively, leading to an effective total bond order of 3.48, comparable to that seen for the Re dimer. The Cr system is different, however. As is expected for a first-row transition-metal system, the ground state of $\text{Li}_4[\text{Cr}_2(\text{CH}_3)_8]$ is more multiconfigurational than in the Re, W, and Mo cases, with the main configuration having a weight of 0.43. The effective bond orders for the σ , π , and δ bonds are 0.71, 1.43 and 0.31, respectively, resulting in a 2.45 effective total bond order (i.e., a greatly reduced bond order compared to that of the Re, W, and Mo dimers).²⁵

Conclusions

Our primary goal when we started this study was to provide a theoretical understanding of the apparently linear

relationship between metal–metal bond length and $\delta \rightarrow \delta^*$ excitation energy for the octamethyldimetalates of Re, Cr, Mo, and W. As our results demonstrate, these seemingly simple anionic systems represent a surprising challenge to modern electronic structure methods, largely because of the difficulty in modeling systems that have large negative charges without electronegative ligands. Nevertheless, by using the CASPT2 method with Li^+ counterions for the Mo, Cr, and W cases, we have been able to model the ground-state geometries of the complexes with either excellent agreement with experiment (Re) or satisfactory agreement (Mo, Cr, and W). This multiconfigurational approach, which is critical for the calculation of excited-state energies of the complexes, does a fairly good job of modeling the trends in $\delta \rightarrow \delta^*$ excitation energy with metal–metal bond length, although the accuracy is such that we are not yet able to explain fully the linear relationship discovered by Sattelberger and Fackler.¹¹

Future progress on these systems will require better ways to accommodate the highly negative charges, such as utilization of the AIMP method in conjunction with the multiconfigurational calculations. These efforts are ongoing.

Acknowledgment. This work has been supported by the Italian Ministero dell'Istruzione dell'Università e della Ricerca. We thank G. La Manna and B. O. Roos for useful discussions.

IC0504061

(25) We note that $[\text{Li}(\text{THF})_4][\text{Cr}_2(\text{CH}_3)_8]$ is cleaved with tetramethylethylenediamine to give $[\text{Li}(\text{TMEDA})_2][\text{Cr}(\text{CH}_3)_4]$. See: Hao, S.; Song, J.-I.; Berno, P.; Gambarotta, S. *Organometallics* **1994**, *13*, 1326.